Environ Monit Assess (2018) 190: 706
https://doi.org/10.1007/s10661-018-7079-3

The development of an overlay model to predict soil salinity risks by using remote sensing and GIS techniques: a case study in soils around Idku Lake, Egypt

Rasha M. Abou Samra · R. R. Ali

Received: 17 August 2018 / Accepted: 30 October 2018 / Published online: 8 November 2018

Abstract Soil salinization is one of the major environmental problems facing agricultural lands in arid and semiarid areas of the world because of its detrimental impacts on agricultural production and on the sustainable development of land resources. Hence, predicting soil salinity is essential to avoiding further soil degradation. The present study is intended to develop a model for predicting soil salinity in soils around Idku Lake by using remote sensing and geographic information system techniques. This lake is a shallow brackish basin located in the western part of the Nile Delta. For this purpose, Landsat 8-OLI images and shuttle radar topography mission 1Arc-Second Digital Elevation Model data were utilized in this research. A total of 91 surface samples were collected across the study area at a depth between 0 and 30 cm and were analyzed via traditional laboratory analysis methods. Five environmental parameters were used in the design of the soil salinity model. A pairwise comparison matrix was used to calculate the factor weight value for each of the layers. A linear regression model was used to plot the relationship between the EC value and raster value of the salinity map derived from the overlay model. According to the results obtained from a pairwise comparison of the factor layers, water table level was the greatest influential factor of soil salinity, followed by landforms. The validation of the model demonstrated a high degree of correlation ($R^2 = 0.72$) between the measured EC values and the salinity values derived from the model. Furthermore, this model could be a useful tool for predicting soil salinity with a suitable validation.

Keywords Electrical conductivity · Overlay salinity prediction model · GIS · NDVI · Environmental parameters

R. M. Abou Samra (✉)
Environmental Sciences Department, Faculty of Science, Damietta University, PO Box 34517, New Damietta City, Egypt
e-mail: rasha.mohamed67@yahoo.com

R. R. Ali
Soils and Water Use Department, National Research Centre (NRC), Cairo 12311, Egypt
e-mail: bediertop@yahoo.com

Introduction

Soil salinization of irrigated agricultural lands is a global environmental problem affecting the sustainable usage of land resources, environmental health, agricultural production, and food security. This process of salinization ultimately results in soil degradation (Gorji et al. 2015; Zewdu et al. 2017). Soil salinization is spreading due to agricultural expansion and climate change, especially in arid and semiarid climatic zones (Jiang et al. 2017). Excess salt concentrations lead to other soil degradation features, such as sealing, crust formation, structural changes, and soil dispersion that leads to soil compaction (Farifteh et al. 2007). Salt-affected soils are generated by high accumulations of salt at the soil surface. Geological

formations such as limestone, halite, shale, and gypsum are the major sources of the accumulated salt. The disparity of soil salinity is influenced by the soil type, parent material, and topography (Clay et al. 2001).

Soil salinity is classified into two main categories: natural primary salinity or human-induced secondary salinity (Allbed and Kumar 2013). Human-induced salinity influences approximately 20% of irrigated lands and 2% of dry lands worldwide (Sharma and Singh 2017). Primary soil salinity exists in regions where the parent material has a great amount of salt (mostly the chlorides of sodium, calcium, and magnesium and, to a minor extent, carbonates and sulfates), the level of the water table is high, and evapotranspiration rates are higher than precipitation rates. However, secondary soil salinity is correlated with insufficient drainage and poor water quality in irrigated areas (Ammari et al. 2013; Arora 2017).

Due to excess soluble salts in saline soils, electrical conductivity (EC) values ≥ 4 dS m^{-1} are observed. This influences plant growth in saline soils, which is usually related to the specific ion toxicity and osmotic stress (Sharma and Singh 2017).

Many soils vary spatially and temporally to a large degree and this affects the assessment of soil salinity. In addition, the traditional laboratory methods for assessing salinity of soil are costly and time-consuming methods, especially since a lot of samples are needed to detect soil salinity (Aldabaa et al. 2015). Also, the EC is often used to express soil salinity. Many factors such as water holding capacity and soil texture influence the use of EC measurements to assess soil salinity (Pozdnyakova and Zhang 1999). Additionally, soil extracts are often used in the determination of EC. The real extract ratios utilized in traditional analysis vary extremely and it is complicated to convert the results into field water content values (Adiku et al. 1992). This has led to the use of various remote sensing and modeling applications for directly detecting, monitoring, and predicting salt-affected regions.

Remote sensing (RS) imagery is an effective approach to map soil salinity. RS can supply helpful information about evapotranspiration, precipitation, and crop types that could be considered indirect indications of soil salinity. Saline areas are often recognized via the existence of patchy white spots of precipitated salts, which can be recorded by RS imagery (Shahid 2013). There are two limitations of the usage of RS data in detecting saline areas. The first limitation is the difficulty in identifying subsurface saline areas due to the lack of resolution in inexpensive RS data (Furby et al. 1995). The second limitation is plant cover of saline soils that blocks the direct detection of the soil (Shahid 2013). Remote sensing and GIS techniques have been widely used to detect, map, and model salt-affected soils (Peng 1998; Farifteh et al. 2006; Allbed and Kumar 2013; Jiang et al. 2017).

Modeling is an important mathematical tool when predicting soil salinity-related dependent variables that assist in decision making. Additionally, model results help in assessing probable scenario analyses. The input data required to run the model differs in complexity according to the data output requirements (FAO 2009). Modeling techniques have been widely used to detect, map, and model salt-affected soils. Corwin et al. (1989) developed three regression models to predict soil salinity potentials. They found a good correlation between soil salinity predicted from the models and the measured salinity in the field. In addition, Lesch et al. (1995) applied a multiple linear regression models to predict soil salinity. Recently, Fourati et al. (2015) applied Partial Least Square Regression (PLSR) model to predict soil salinity. The model gives a coefficient of determination $R^2 = 0.52$ using the linear regression.

The development of soil salinity on agricultural lands can commonly be related to many environmental factors: depth to water table, soil texture, geology, landforms, and vegetation density. Depth to water table is one of the most important factors in the development of soil salinity because shallow water table would enhance the movement of salts to the surface of the soil (Corwin et al. 1989). Stressed vegetation can be an indirect indication of the existence of excess salts in the soils. Saline soils are commonly recognized by identifying poorly vegetated regions (Asfaw et al. 2016). Mokarram et al. (2015) studied the relationship between soil salinity and landforms by using multiple regression analysis. They found that sand content in the top soils was the greatest influential factor in the prediction of soil salinity. To compare two factors with each other for their relative importance in predicting the soil salinity susceptibility, multi-criteria evaluation was used in conjunction with pairwise comparison matrix (PWCM). Multi-Criteria Evaluation (MCE) is a method that can be used to evaluate and weight variables regarding their importance to achieve a particular objective which helps in a decision-making process (Alvarado et al. 2016).

The present study was planned to assess the extent of soil salinity in areas around Idku Lake and to map the spatial distribution of the problem through developing an overlay model based on environmental factors, RS data, and field measurements of EC. For this purpose, a semi-comprehensive survey was carried out over the research area so as to obtain an estimation of the soil patterns.

Materials and methods

Study area

The study area, which covers more than 1000 km^2, is located in the western part of the Nile Delta, extending from 30° 26′ 45″ N to 30° 59′ 15″ N and from 29° 51′ 30″ E to 30° 31′ 08″ E (Fig. 1), around Lake Idku. This lake is a shallow brackish basin located in the western part of the Nile Delta and has an area of approximately 126 km^2 (Ali and Khairy 2016). This area is characterized by a hot desert climate, calmed by blowing winds from the Mediterranean Sea. August is the warmest month, with an average temperature of 20.42 °C. The average temperature in January is 13.15 °C. June is the driest month, with 0 mm of rainfall. Most precipitation occurs in January, with an average of approximately 23.8 mm. The average temperatures differ by approximately 13.4 °C during the year. The evaporation can range from 3.3 to 4.8 mm/day with an average of 4.25 mm/day (Zaki and Swelam 2017). According to the US Soil Taxonomy System (USDA 2014), the soil temperature regime would be identified as "Thermic" since the average annual temperature is not more than 21 °C. Also the soil moisture regime would be defined as "Torric" where the rainfall is always lower than evaporation rates (more than 180 days).

The soil texture in this area is recognized as clayey soils with recently reclaimed sandy soils (El-Dars et al. 2014). The slope of soil surface is flat. Soil depths differ considerably, ranging from moderately deep to deep, and well match the water table depths. Soil colors range from dark grayish brown to yellow (Hegab 2014).

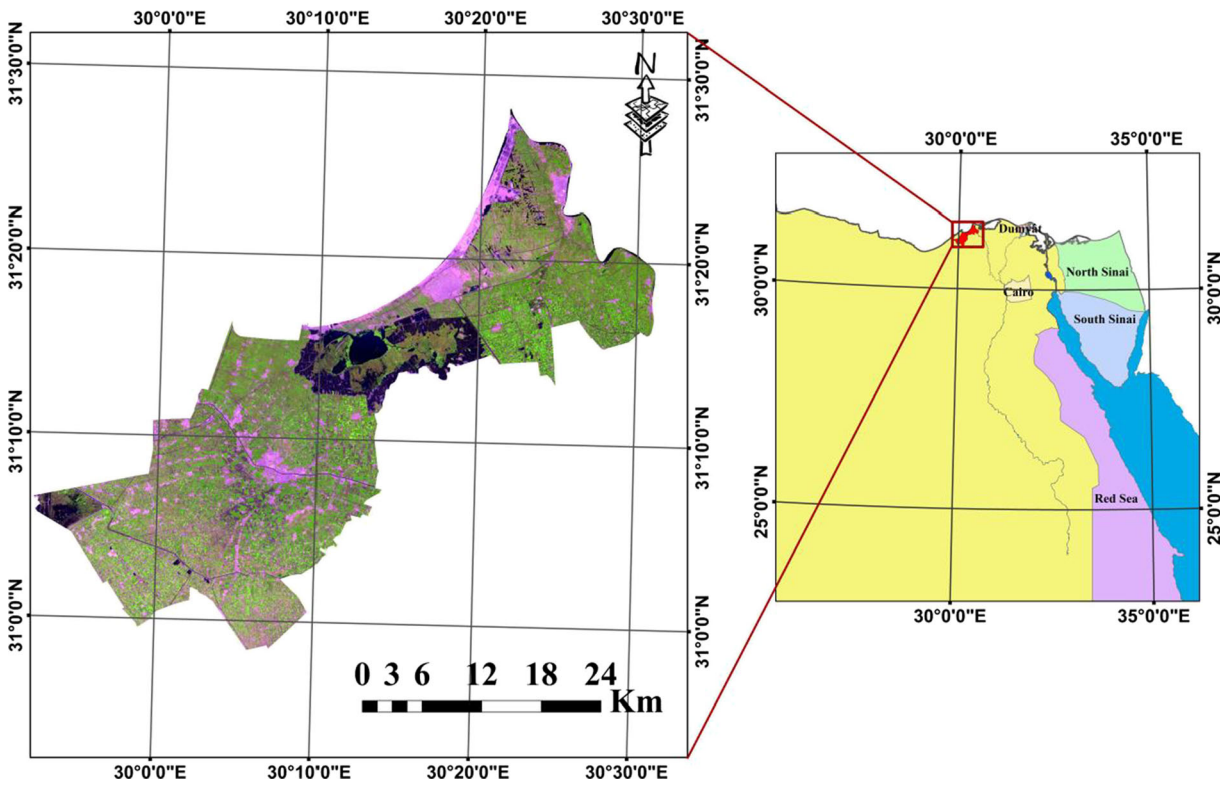

Fig. 1 A spatial location of the study area

Data acquisition and processing

The present study was performed by using two multispectral Landsat 8-OLI images (path 177/rows 38 and 39). The images were acquired on 1 September 2015 with a spatial resolution of 30 m. These images are free of sensor imperfections and clouds. The Landsat images were obtained in the GeoTIFF format from the United States Geological Survey (USGS) site (http://earthexplorer.usgs.gov/). By using ENVI 5.1 software, images were projected onto a UTM coordinate system using WGS 1984 datum assigned to UTM zone 36. The atmospheric correction was done to reduce the noise effect using the FLAASH Model (Perkins et al. 2005), which can correct both collective and multiplicative atmospheric effects (Wu et al. 2014), then the images were mosaicked. Analysis of the images was accomplished by using ENVI 5.1 and Arc-GIS 10.3 software for image processing, analyzing, and presenting the results.

Geologic and geomorphological units of the study area

The shuttle radar topography mission (SRTM) could be combined with multispectral images (Landsat 8-OLI) to realize better view of the landscape, as it provides better functionalities than the topographic maps. To delineate the landform units, the SRTM images with a spatial resolution of 30 m were downloaded from the USGS site (http://earthexplorer.usgs.gov/). The digital elevation model (DEM) of the study area was extracted from SRTM by using Arc-GIS 10.3 (Fig. 2). The SRTM is an esteemed space data of earth surface acquired by precise radar scanning land at 1-arc sec intervals (Ali and Shalaby 2012). The Landsat 8-OLI image and SRTM data were processed in ENVI 5.1 software to identify the different physiographic units according to the approach developed by Dobos et al. (2002). The map legend was designed according to Zinck and Valenzuela (1990). The interpretation of Landsat 8-OLI and SRTM images generates preliminary landform units which were verified during field work.

Salinity model from measured EC

Soil field survey and laboratory analyses

A total of 91 sites were investigated in the field to collect surface soil samples (0–30) during September 2015. The samples were collected using grid system (3 ×

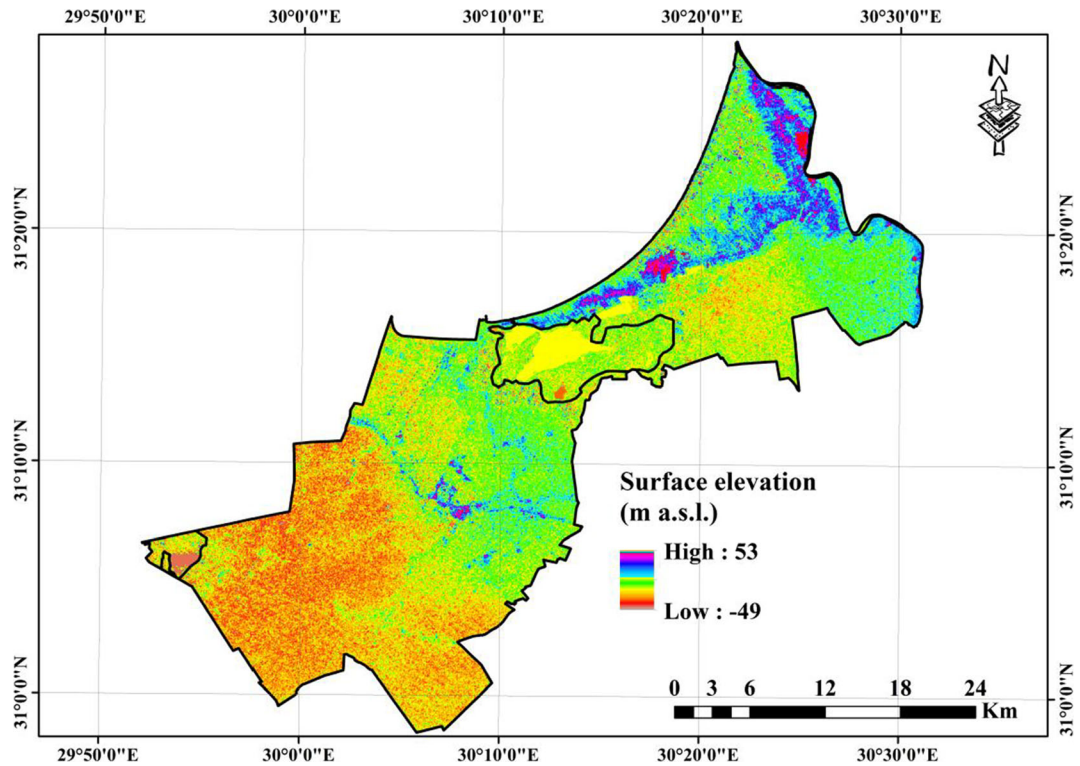

Fig. 2 Digital elevation model (DEM) of the study area as derived from the SRTM 1 arc-second data

3 km), and some sites were shifted to avoid urban areas and water bodies. Positions were located by global positioning system (GPS). An appropriate number of samples were selected to represent all landforms in consonance with their areas. Figure 3 shows the locations of the surface soil samples. All soil samples were air-dried and sieved through a 2-mm mesh. EC is often used to express soil salinity. EC was measured in a 1:2.5 soil-water extract for coarse-textured soils, while it was measured in saturated paste extract for fine-textured soils. The EC was measured via an electronic bridge. The samples were analyzed using the soil survey laboratory methods manual (USDA 2004).

Spatial distribution of soil properties

Spatial interpolation is a well-known method used to estimate the values of unknown locations based on the characteristics of known data sets. The inverse distance-weighted (IDW) method is a type of the interpolation method, which estimates the values of unmeasured locations using a linear combination of the surrounding known points weighted by the mean distance from them to the unknown point (Yin et al. 2012; Chen and Liu 2012; Chen et al. 2016). The IDW algorithm of Arc-GIS 10.3 was used to interpolate the measured EC values over the study area. According to FAO (1988), EC values were used to classify the levels of soil salinity.

Soil salinity risk prediction model

Environmental parameters

Environmental parameters were used in the design of soil salinity risk model. These parameters include water table level, soil texture, landforms, geology, and vegetation density. The water table level was determined by using PVC pipe and measuring stick. In this regard, spline method was used in the interpolation of water table data. It is one of the methods of interpolation that estimates values via mathematical function that reduces surface bend (Robinson and Metternicht 2006). Soil texture was determined by the percentage of sand, silt, and clay following the soil survey laboratory methods manual (USDA 2014). The standard pipette procedure was applied for fine-textured soils, whereas dry sieving procedure was utilized for coarse-textured samples.

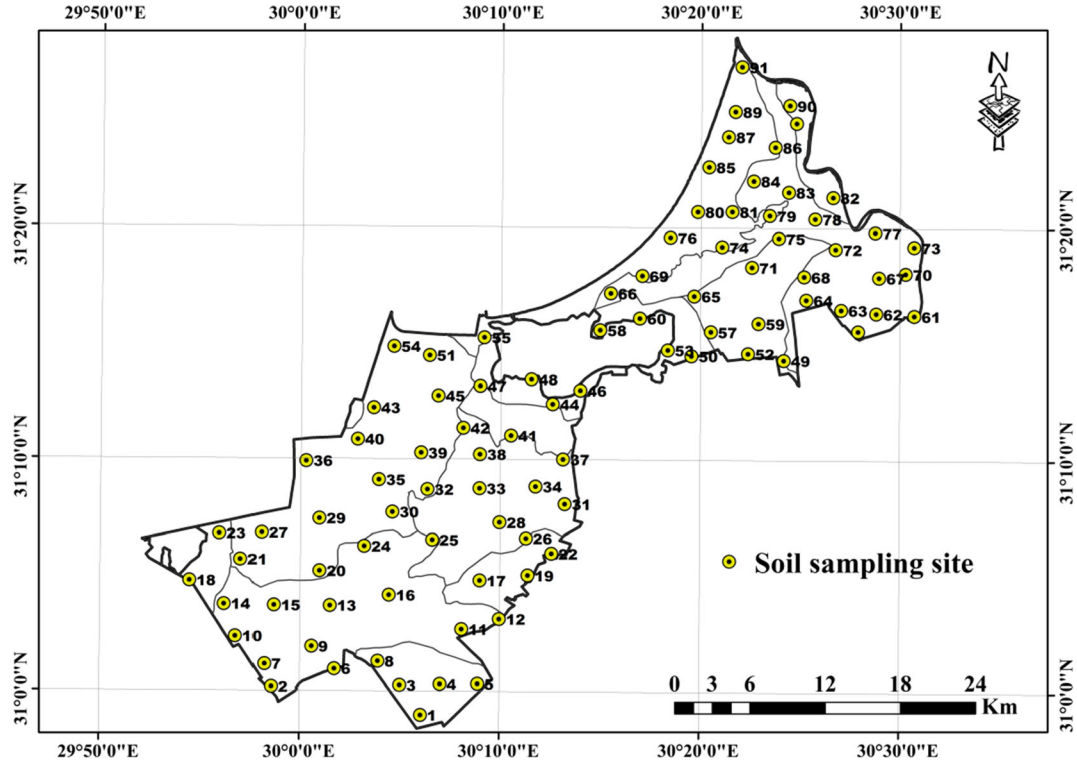

Fig. 3 Locations of soil samples over the investigated area

The geological units of this study area were extracted from the geological map of Egypt (scale 1:500,000) produced by CONOCO (1989).

DEM is a three-dimensional model of the earth's surface elevation (Brough 1986); it can be utilized to display sets of data which can help in landform's mapping (Ali and Moghanm 2013). Information extracted from DEM, such as surface elevation, could be utilized with the Landsat images to enhance their competence for soil mapping (Lee et al. 1988). DEM and Landsat 8-OLI images were used to identify and delineate the landform units that were checked and modified during field work.

To extract the vegetation density layer from Landsat 8-OLI satellite image, the normalized differential vegetation index (NDVI) was used. NDVI is the most popular used index for spotlighting vegetation regions on satellite images (Gandhi et al. 2015). It can detect worthy information about the condition of vegetation cover, vegetation structure, and leaf distribution (Yengoh et al. 2014). The NDVI was calculated from the following equation (Mokarram et al. 2015):

$$\mathrm{NDVI} = (\mathrm{NIR}-\mathrm{R})/(\mathrm{NIR}+\mathrm{R}) \quad (1)$$

The value of this index ranges from −1 to 1. The NDVI map derived from the equation is shown in Fig. 4.

The raster of the factor layers is on different resolutions. Before applying the model, all the layers were resampled to the same cell size (30 m) using resample tool in Arc-GIS. All the factor layers were with a spatial resolution of 30 m. All the layers of the environmental parameters were reclassified into four classes according to their susceptibilities to soil salinity risks via the reclassify tool in Arc-GIS 10.3 software, where class 1 represents the lowest susceptibility to soil salinity and class 4 represents the highest. The used ranks for water table level, landform, soil texture, geology, and vegetation density are represented in Table 1.

Assigning weight of factors and multi-criteria evaluation

The multi-criteria evaluation approach was used in weighted overlay analysis. Using a PWCM, the factor weight values for each of the layers were calculated by comparing two factors with each other for their

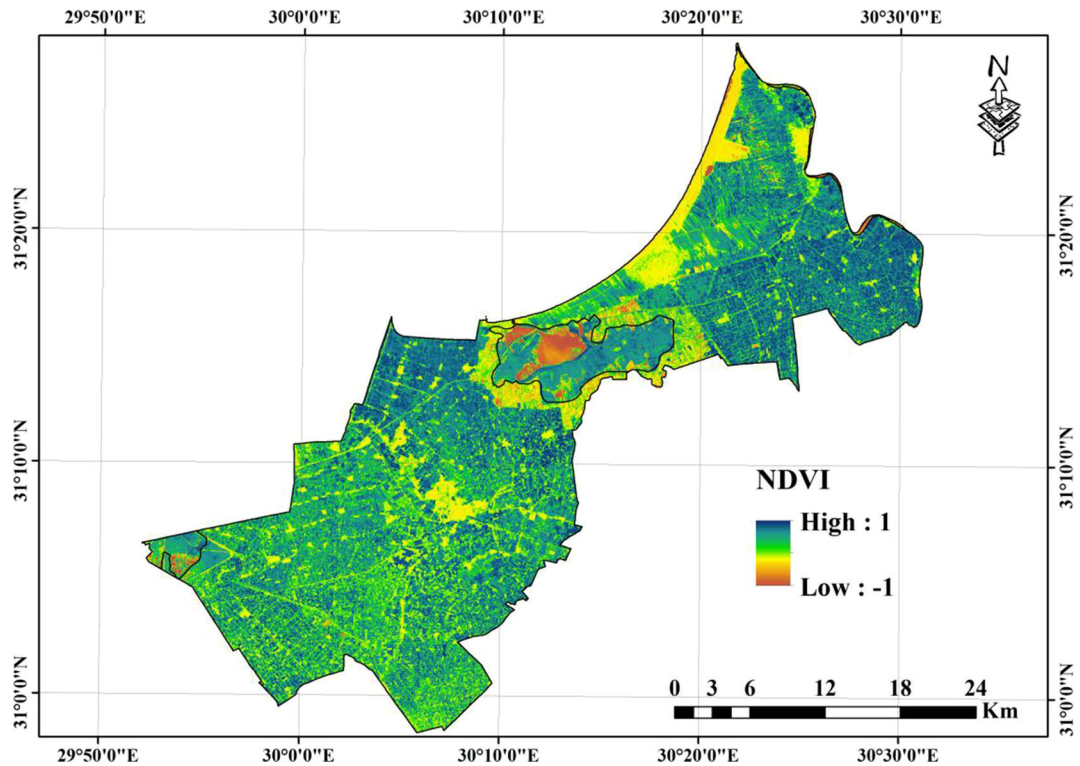

Fig. 4 Normalized difference vegetation index (NDVI)

Table 1 Ranks used for water table level, landform, soil texture, geology, and vegetation density, according to their susceptibilities to soil salinity risks

Rank	Salinity class	Water table level (cm)	Landform	Soil texture	Geology	Vegetation density
1	None to slightly saline	160	Coastal sand sheet River terraces Overflow basin River levee Decantation basin River Nile	Sandy	Nile silt	0.63–1
2	Moderately saline	90	Former lake bed	Sandy loam	Marine deposits	0.35–0.62
3	Strongly saline	60	Fish ponds	Sand clay loam	Lacustrine deposits	− 0.05 to 0.34
4	Very Strongly saline	50	Lake	Loam Clay loam Clay	Water bodies	− 1 to − 0.051

relative importance in predicting the soil salinity susceptibility of the study area. The scale formulated by Saaty (1980) was utilized in the application of PWCM. The values of the scale range from 9 to 1/9. A ranking of (1, 3, 5, 7, 9) shows that the row factor is more significant in comparison with the column factor, whereas a ranking of (1/3, 1/5, 1/7, 1/9) shows that the row factor is less significant than the column factor (Kihoro et al. 2013). A value of (1) indicates that the row and column factors have the same significant. The weights of all layers sum to one. Weight output from pairwise comparison matrix for each of the factor layers is shown in Table 2.

Once the layers and their weights were obtained, weighted overlay analysis was applied using Arc-GIS 10.3 by multiplying the cell value of every environmental parameter by its particular weight to produce a map of soil salinity levels (Eq. 2). In the output raster, four classes were obtained from the model, ranging from 1 to 4, where the higher raster class 4 represented the regions with high salinity levels, while the lower raster class 1 represented regions with low salinity levels.

$$\begin{aligned}\text{Salinity} = {} & (0.41 \times \text{water table level}) \\ & + (0.24 \times \text{landforms}) \\ & + (0.19 \times \text{soil texture}) \\ & + (0.11 \times \text{geology}) \\ & + (0.05 \times \text{vegetation density}) \end{aligned} \quad (2)$$

Validation and comparison of the soil salinity risk maps

The validation and comparison of the soil salinity risk maps derived from the measured soil EC and the overlay soil salinity risk model of the five factor layers were performed. A linear regression model in Excel 2013 was used to plot the relationship between the EC values and raster values of the salinity map derived from the overlay model on the scatter diagram. Then, the correlation (R^2) between the EC values and raster values of the model was obtained (modified per Zewdu et al. 2017). A flow chart of the methodology is shown in Fig. 5.

Table 2 Pairwise comparison of factor layers

Layer/factor	Water table level	Land form	Geology	Soil texture	Vegetation density	Criteria weights (W)
Water table level	1.00					0.49
Landform	1/5	1.00				0.20
Geology	1/3	1/3	1.00			0.18
Soil texture	1/3	1/7	1/5	1.00		0.09
Vegetation density	1/7	1/5	1/7	1/7	1.00	0.04

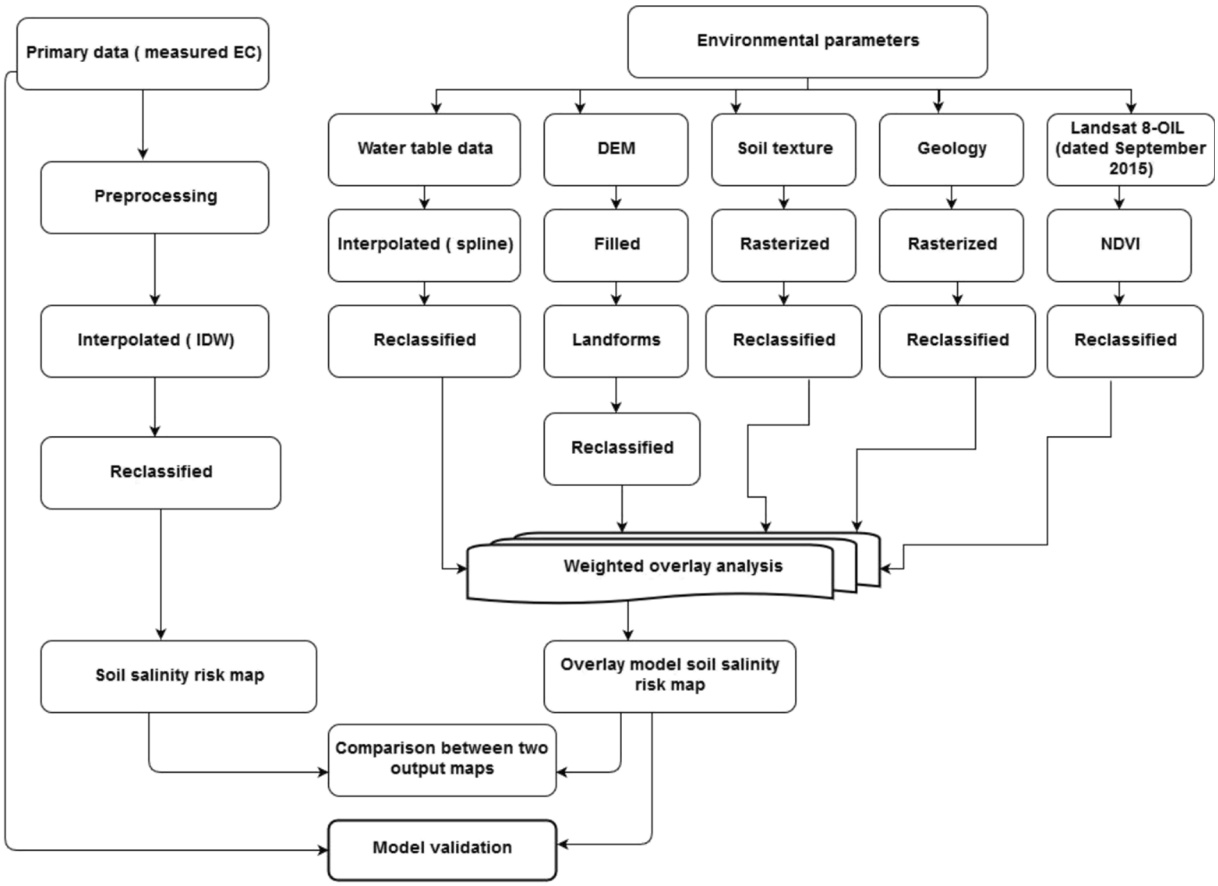

Fig. 5 Flow chart of methodology showing the steps used in this work (modified after Zewdu et al. 2017)

Results and discussion

Geologic and geomorphological units of the study area

Landsat 8-OLI, SRTM images, and field data were used to delineate the landform units. The results showed that there are three main landforms in the study area: the floodplain, the lacustrine plain, and the marine plain (Fig. 6). The main landform in this area is the floodplain, which occupies an area of 746.89 km^2 (73.45% of the total study area). The sedimentary Nile depositions contributed to developing the floodplain (Islam 2016). Approximately 16.19% of this area is covered by the lacustrine plain (164.65 km^2). The lacustrine plain was formed by the deposition of sediment entering the lake. After sediment deposition, the water may be drained from the lake via evaporation or other processes, which leaves the sediment behind (Thornbury 1950). The marine plain is found in the northern portion of the study area and occupies an area of 105.37 km^2 (10.36% of the total study area). The marine plain is characterized by a flat and low-lying area close to the seacoast (Ali and Moghanm 2013). Three geological units are recognized underlying the study area, including lacustrine deposits, marine deposits, and Nile silt, which are shown in Fig. 7. The Nile silt dominates the largest section of the study area, covering 735.28 km^2 (72.25% of the total study area). The lacustrine and marine deposits occupy approximately 16.59 and 1.26% of the total study area, respectively.

Spatial distribution of soil properties

Tables 3 and 4 illustrate some physical and chemical characteristics of the investigated soils. The spatial distribution of the EC over the study area is illustrated in Fig. 8. The EC values in the topsoil (0–30 cm) range from 0.43 to 24.38 dS/m. It was observed that higher EC values are found in locations which are characterized by shallow water table because it encourages the movements

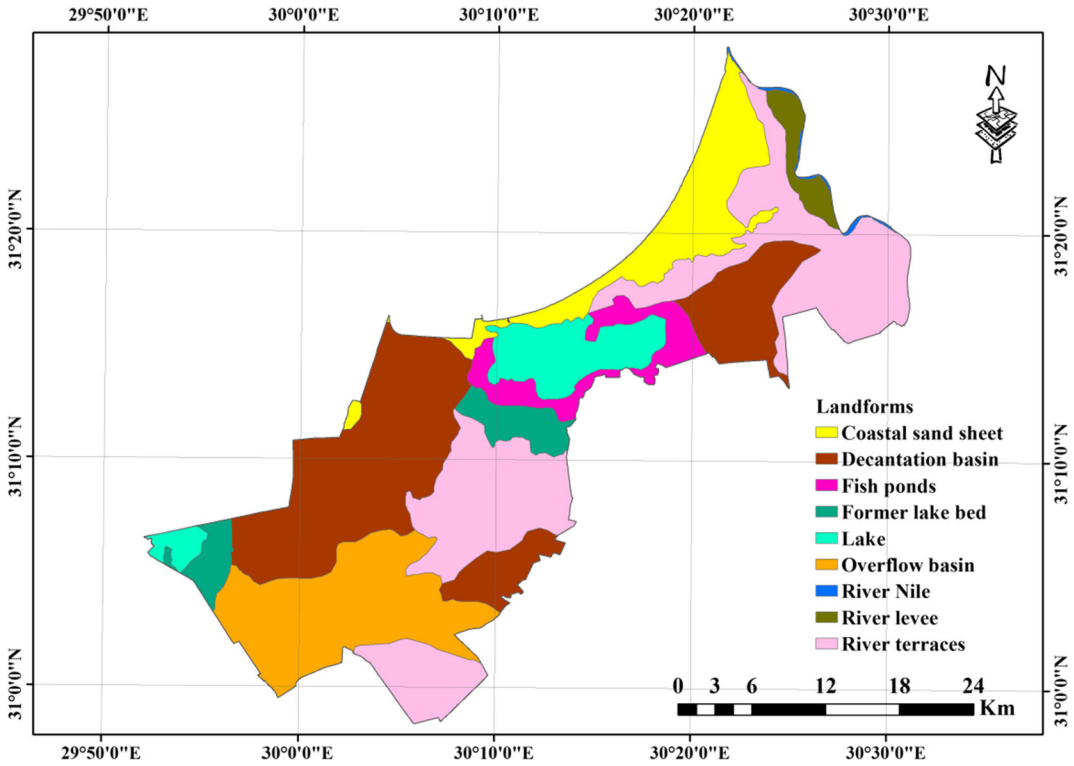

Fig. 6 Landforms of the study area

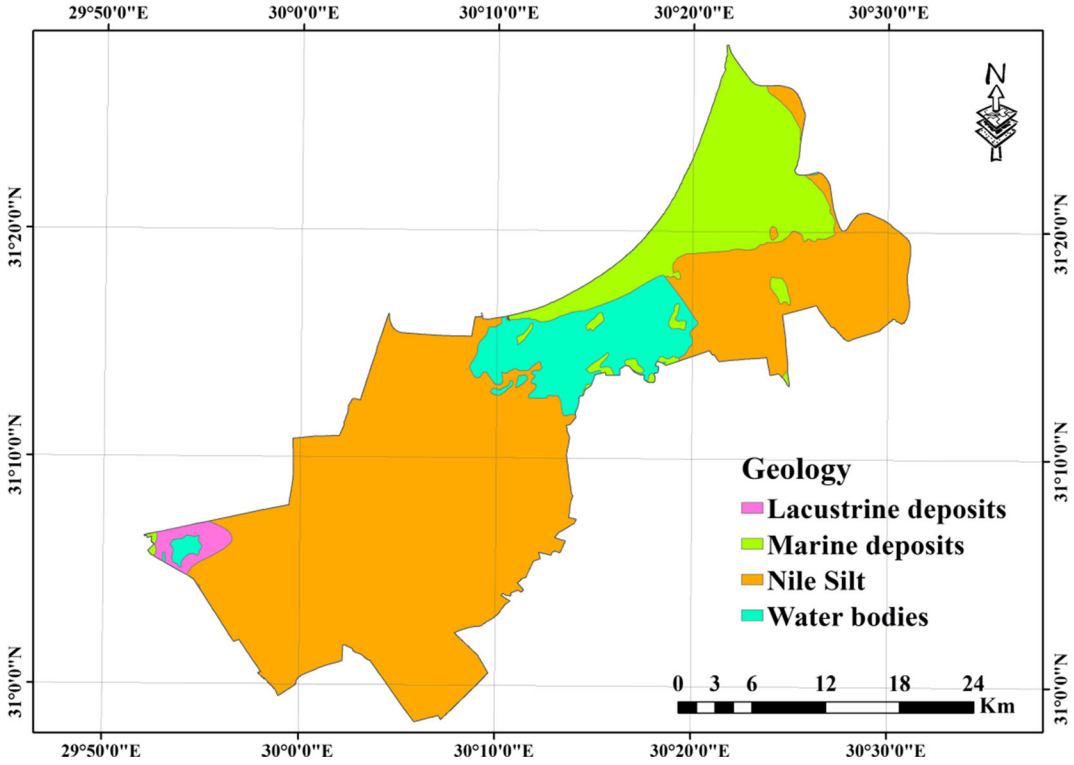

Fig. 7 Geological units of the study area

Table 3 Some chemical and physical characteristics of the studied soil profiles

Profile no.	EC (dS m^{-1})	Water table level (cm)	Soil texture	Landforms	Profile no.	EC (dS m^{-1})	Water table level (cm)	Soil texture	Landforms
1	0.56	140	C	River terraces	47	19.32	50	L	Fish ponds
2	2.44	100	SCL	Overflow basin	48	22.37	40	L	Fish ponds
3	0.44	130	C	River terraces	49	2.15	130	C	Decantation basin
4	0.75	140	C	River terraces	50	18.71	50	L	Fish ponds
5	0.65	150	C	River terraces	51	3.4	70	SL	Decantation basin
6	2.3	120	SCL	Overflow basin	52	2.55	80	C	Decantation basin
7	2.5	90	SCL	Overflow basin	53	24.38	40	L	Fish ponds
8	1.1	100	C	River terraces	54	1.25	100	SL	Decantation basin
9	1.6	90	SCL	Overflow basin	55	12.51	40	SL	Coastal sand sheet
10	3.5	80	SCL	Overflow basin	56	1.35	120	C	River terraces
11	1.2	110	C	Overflow basin	57	8.47	60	L	Decantation basin
12	1.3	120	C	Overflow basin	58	22.61	40	L	Fish ponds
13	2.84	90	SCL	Overflow basin	59	0.84	80	C	Decantation basin
14	18.42	60	SL	Overflow basin	60	12.62	40	L	Fish ponds
15	11.2	70	SCL	Overflow basin	61	0.81	100	CL	River terraces
16	3.66	110	C	Overflow basin	62	0.56	120	CL	River terraces
17	4.31	130	C	Decantation basin	63	1.13	120	CL	River terraces
18	21.5	40	SL	Former lake bed	64	1.46	130	CL	River terraces
19	2.11	140	C	Decantation basin	65	5.46	70	L	Decantation basin
20	3.33	90	SCL	Decantation basin	66	5.66	50	S	River terraces
21	22.5	60	SL	Decantation basin	67	0.68	100	CL	River terraces
22	2.22	150	C	Decantation basin	68	1.43	130	CL	River terraces
23	20.71	50	SL	Former lake bed	69	2.33	120	S	Coastal sand sheet
24	1.8	100	SCL	Overflow basin	70	0.63	100	CL	River terraces
25	1.4	120	C	Overflow basin	71	1.88	110	CL	Decantation basin
26	1.22	140	C	River terraces	72	0.47	110	CL	River terraces
27	5.34	70	SL	Decantation basin	73	0.44	100	CL	River terraces
28	0.56	120	C	River terraces	74	2.21	120	S	Coastal sand sheet
29	2.36	80	SCL	Decantation basin	75	1.62	120	S	Decantation basin
30	3.21	100	SCL	Decantation basin	76	1.42	110	S	Coastal sand sheet
31	3.27	140	C	River terraces	77	0.54	110	CL	River terraces
32	4.33	100	C	Decantation basin	78	0.68	110	CL	River terraces
33	3.84	100	C	River terraces	79	0.87	120	S	Coastal sand sheet

Table 3 (continued)

Profile no.	EC (dS m^{-1})	Water table level (cm)	Soil texture	Landforms	Profile no.	EC (dS m^{-1})	Water table level (cm)	Soil texture	Landforms
34	1.2	110	C	River terraces	80	2.35	100	S	Coastal sand sheet
35	2.4	120	SCL	Decantation basin	81	2.11	120	S	Coastal sand sheet
36	3.66	90	SL	Decantation basin	82	0.48	100	C	River levee
37	2.11	90	C	River terraces	83	0.43	110	SL	River terraces
38	3.89	90	C	River terraces	84	1.54	120	SL	River terraces
39	2.45	90	L	Decantation basin	85	1.36	120	S	Coastal sand sheet
40	2.65	80	SL	Decantation basin	86	0.47	120	SL	Coastal sand sheet
41	6.48	80	L	Decantation basin	87	1.58	120	S	Coastal sand sheet
42	6.12	80	L	River terraces	88	1.22	100	SL	River levee
43	2.26	100	SL	Decantation basin	89	1.31	100	S	Coastal sand sheet
44	18.37	50	L	Fish ponds	90	0.43	100	SL	River levee
45	1.55	70	L	Decantation basin	91	1.06	90	S	Coastal sand sheet
46	18.33	50	L	Fish ponds					

C clay, *SCL* sandy clay loam, *SL* sandy loam, *S* sandy

Table 4 Some statistical characteristics of the investigated soils

Properties	Total samples	Mean	Maximum	Minimum	SD
Water table level cm)	91	96.92	150	40	28.66
EC (dS m^{-1})	91	4.69	24.38	0.43	6.43

of salts up to the surface of the soil. In addition, the high EC values were detected in soils around Idku Lake, predominantly in the landforms of fish ponds and the former lake bed. The results indicated that the soil salinity varies excessively over this area (SD = 6.43). Note that the EC values increase toward Idku Lake. This increase may be due to the leakage from the saline Idku Lake into neighboring areas, which enhance the shallow groundwater level (Hegab 2014). The soil depth ranges from 40 to 150 cm, with a mean value of 96.92 cm. The soil textures vary from clayey to sandy soils. The variation in soil texture may be due to the variations of soil topography, parent material, the degree and type of weathering, and the mechanism of transportation (Abd-Elgawad et al. 2013; Hegab 2014). The results of the present study are consistent with those of a previous study by Ali and Moghanm (2013) that used GIS and RS techniques to identify the differences in soil properties over the landforms of the dry regions around Idku Lake. They found that the EC values ranged between 0.1 and 51 dS/m in the topsoil layer. They also detected that marine and lacustrine deposits generally showed the highest EC values. In addition, the results of this work coincide with the results obtained by Hegab (2014), who examined the limitation of soil fertility in soils close to Idku Lake. He observed that the soil depths ranged from moderately deep to deep and the soil ECs ranged from 2.60 to 60.90 dS m^{-1}.

Soil salinity classes derived from measured EC

The map of the soil salinity derived from the IDW interpolation method of the EC values over the study area is divided into four classes of salinity levels according to FAO (1988). The classes are none to slightly saline, moderately saline, strongly saline, and very strongly saline. None to slightly saline soils accounted for the largest area (672.03 km^2), representing approximately 67.22% of the total study area. Moderately saline soils accounted for 11.99% of the total area. It was obvious that the strongly and very strongly saline soils were concentrated in those areas adjacent to Idku

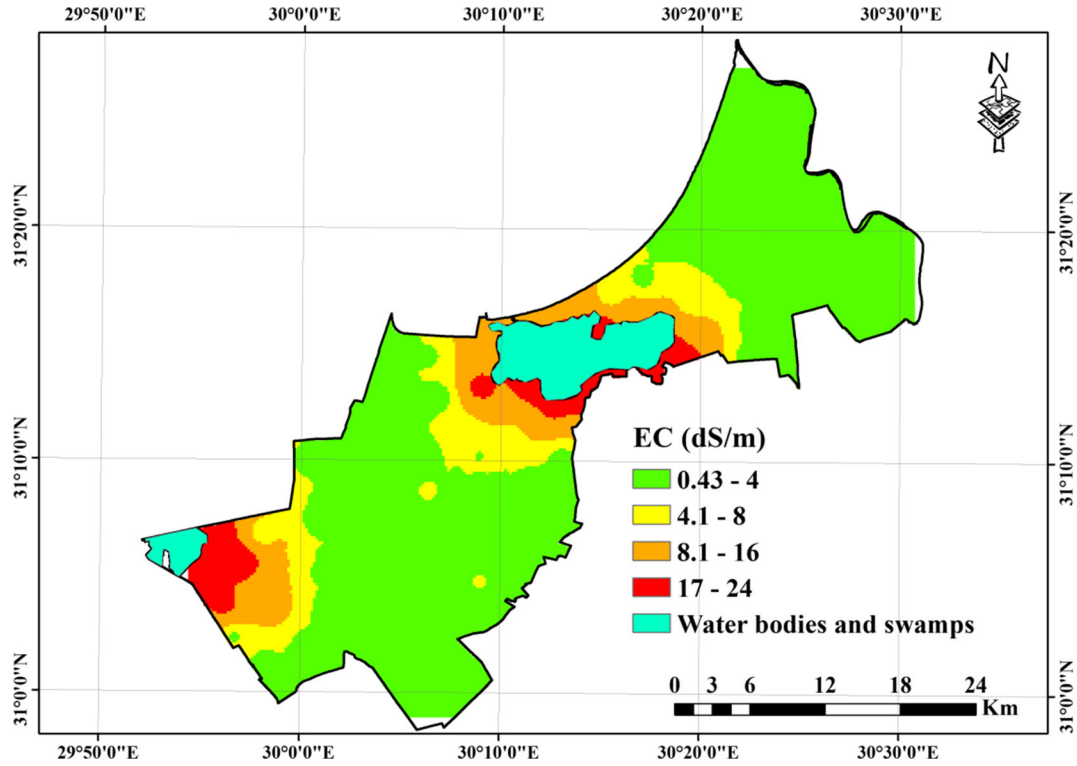

Fig. 8 Spatial distribution of EC over the study area

Lake and covered 11.17 and 9.62% of the total study area, respectively. The spatial extents of the salinity classes derived from the measured EC are shown in Table 5 and Fig. 9a. The class degree clearly increased with proximity to Idku Lake, likely because of the seepage from the lake into nearby areas.

Overlay soil salinity risk prediction model

According to the results obtained from a pairwise comparison of the factor layers influencing the soil salinity, the water table level was the greatest influential factor (49%), followed by landforms (20%). Geology and soil texture had degrees of influence of 18 and 9%, respectively. The vegetation density had the lowest degree of influence (4%). The results of the overlay model represent four levels of soil salinity, which are recognized as none to slightly saline, moderately saline, strongly saline, and very strongly saline. None to slightly saline soils account for the largest extent (614.06 km^2), covering 61.42% of the total area. These areas were characterized by high water table and healthy vegetation lands.

According to the model, moderately saline soils covered 24.14% of the total study area. Strongly saline and very strongly saline soils were concentrated in areas around Idku Lake and accounted for 6.27 and 8.17% of the total study area, respectively. These areas were characterized by shallow water table and low-set lands with poorly vegetation. The areal extents of the salinity classes derived from the overlay model are illustrated in Table 5 and Fig. 9b.

Table 5 The areal extents of the salinity classes derived from measured EC and the overlay model

Salinity level (dS/m)	Salinity class	Area (km^2) measured EC	Area (%) overlay model
> 4	None to slightly saline	672.03	614.06
4–8	Moderately saline	119.85	241.36
8–16	Strongly saline	111.67	62.7
< 16	Very strongly saline	96.23	81.67
	Total	**999.78**	**999.78**

the significance of data presented in bold text

Validation and comparison of the model

The validation of the overlay model displayed a high degree of correlation ($R^2 = 0.72$) between the

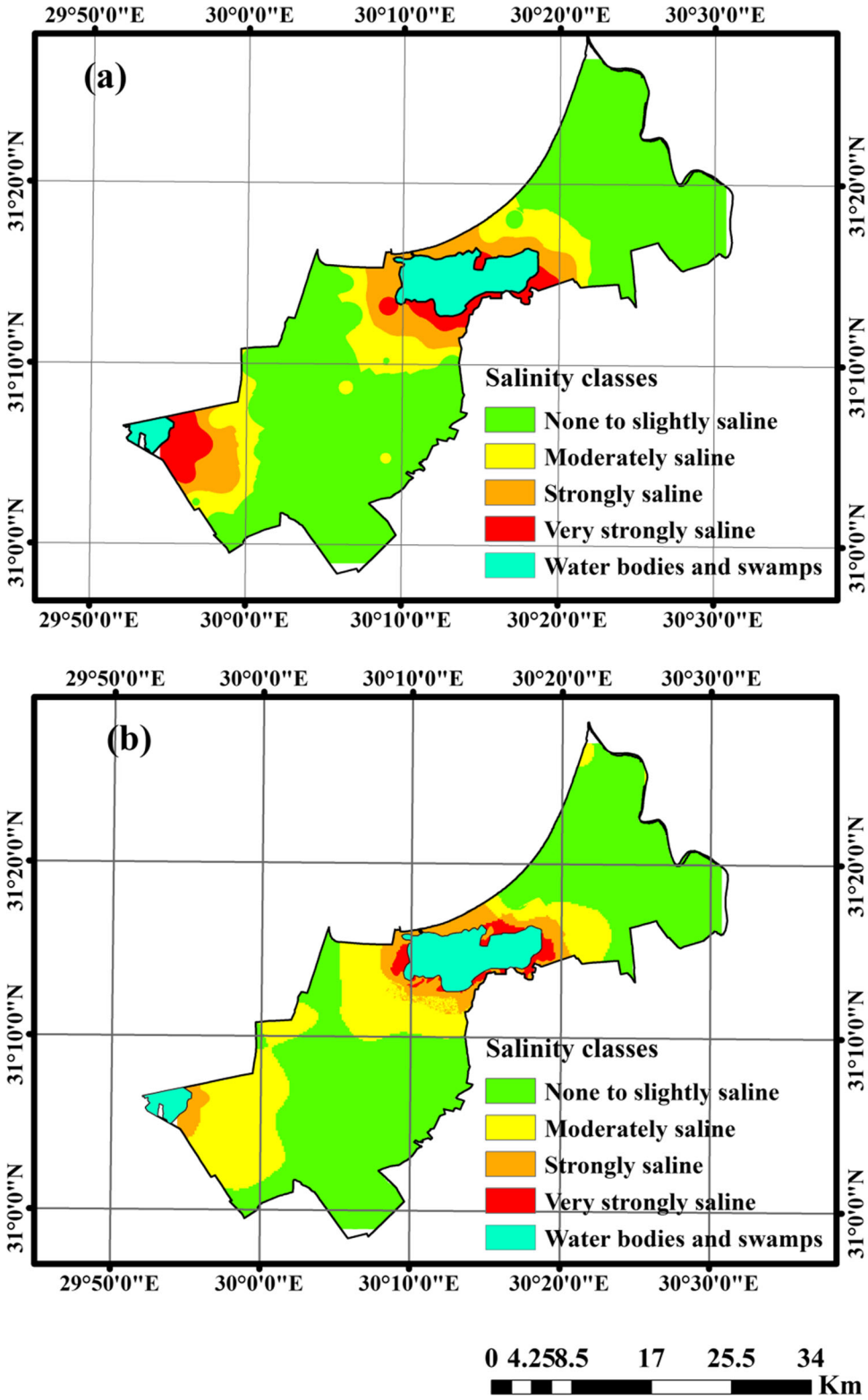

Fig. 9 Soil salinity prediction map derived from **a** measured EC and **b** overlay model

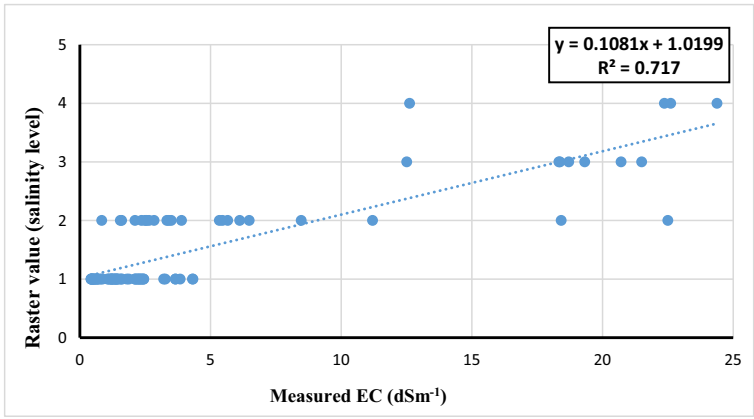

Fig. 10 Regression analysis model between EC vs. raster value of overlay model

measured EC values and the salinity values deduced from the model (Fig. 10).

Remote sensing and modeling techniques have been widely used to detect, map, and model salt-affected soils. Corwin et al. (1988) developed an overlay model to predict soil salinity potential based on four factors (leaching, soil permeability, depth to water table, and groundwater quality). Verification of the model displayed a median success in predicting soil salinity potentials. They recommended that the development of a more advanced model would weigh the significance of each effective factor in soil salinity evolution at a specific location. Also, Akramkhanov and Vlek (2012) utilized a neural network model to predict soil salinity based on environmental parameters in the Aral Sea Basin. They found that about 70–90% of the locations were precisely evaluated. In addition, Yahiaoui et al. (2015) developed a linear regression model to predict that soil salinity relied on elevation in the Lower Cheliff plain (Algeria). The model gives a coefficient of determination $R^2 = 0.45$ using the linear regression. Recently, Yu et al. (2018) used PLSR and Landsat OLI images to map soil salinity in Semiarid West Jilin Province, China. Results showed that the models' accuracy was enhanced by the combination of the reflectance bands and spectral indices.

The model used in this research can predict soil salinity level at any location in the image. As a result, the overlay soil salinity risk model developed from the five environmental factors (groundwater table, landforms, soil texture, geology, and vegetation density) is effective for predicting soil salinity levels.

Conclusion

The findings of the present study predicted the soil salinity levels over the areas around Idku Lake by developing an overlay soil salinity model. Five environmental parameters, including groundwater level, landforms, soil texture, geology, and vegetation density, were used in the design of the soil salinity risk model. The soil salinity levels derived from the model were compared to EC values derived from a conventional laboratory analysis. The validation of the model displayed a high correlation coefficient ($R^2 = 0.73$) between the measured EC values and the salinity deduced from the model. The high degree of correlation makes this model a favorable tool for predicting soil salinity.

Acknowledgements The author deeply acknowledges the comments and revisions of two anonymous reviewers. The author also appreciates the time spent by the reviewers to make this manuscript in this shape.

References

Abd-Elgawad, M., Shendi, M. M., Sofi, D. M., Abdurrahman, H., & Ahmed, A. M. (2013). Geographical distribution of soil salinity, alkalinity, and calcicity within Fayoum and Tamia districts, Fayoum Governorate, Egypt. In *Developments in Soil Salinity Assessment and Reclamation* (pp. 219–236). Springer.

Adiku, S., Renger, M., & Roth, C. (1992). A simple model for extrapolating the electrical conductivity data of gypsum containing soils from reference soil extract data. *Agricultural Water Management, 21*, 235–246.

Akramkhanov, A., & Vlek, P. L. (2012). The assessment of spatial distribution of soil salinity risk using neural

network. *Environmental Monitoring and Assessment, 184*, 2475–2485.

Aldabaa, A., Weindorf, D. C., Chakraborty, S., Sharma, A., & Li, B. (2015). Combination of proximal and remote sensing methods for rapid soil salinity quantification. *Geoderma, 239*, 34–46.

Ali, E. M., & Khairy, H. M. . (2016). Environmental assessment of drainage water impacts on water quality and eutrophication level of Lake Idku, Egypt. *Environmental Pollution, 216*, 437–449.

Ali, R., & Moghanm, F. (2013). Variation of soil properties over the landforms around Idku Lake, Egypt. *The Egyptian Journal of Remote Sensing and Space Science, 16*(1), 91–101.

Ali, R., & Shalaby, A. (2012). Sustainable agriculture in the arid desert west of the Nile delta: a crop suitability and water requirements perspective. *International Journal of Soil Science, 7*(4), 116–131.

Allbed, A., & Kumar, L. (2013). Soil salinity mapping and monitoring in arid and semi-arid regions using remote sensing technology: a review. *Advances in remote sensing, 2*(04), 373–385.

Alvarado, A., Esteller, M., Quentin, E., & Expósito, J. (2016). Multi-criteria decision analysis and GIS approach for prioritization of drinking water utilities protection based on their vulnerability to contamination. *Water Resources Management, 30*, 1549–1566.

Ammari, T., Tahhan, R., Abubaker, S., Al-Zu'bi, Y., Tahboub, A., Ta'Any, R., Abu-Romman, S., Al-Manaseer, N., & Stietiya, M. (2013). Soil salinity changes in the Jordan Valley potentially threaten sustainable irrigated agriculture. *Pedosphere, 23*(3), 376–384.

Arora, S. (2017). Diagnostic properties and constraints of salt-affected soils. Bioremediation of salt affected soils. In *An Indian Perspective* (pp. 41–52). Springer.

Asfaw, E., Suryabhagavan, K., & Argaw, M. (2016). Soil salinity modeling and mapping using remote sensing and GIS: the case of Wonji sugar cane irrigation farm, Ethiopia. *Journal of the Saudi Society of Agricultural Sciences*. https://doi.org/10.1016/j.jssas.2016.05.003.

Brough, P. A. (1986). *Principle of geographical information systems for land resources assessment*. Oxford: Clarendon Press.

Chen, F.-W., & Liu, C.-W. (2012). Estimation of the spatial rainfall distribution using inverse distance weighting (IDW) in the middle of Taiwan. *Paddy and Water Environment, 10*(3), 209–222.

Chen, Y., Shan, X., Jin, X., Yang, T., Dai, F., & Yang, D. (2016). A comparative study of spatial interpolation methods for determining fishery resources density in the Yellow Sea. *Acta Oceanologica Sinica, 35*(12), 65–72.

Clay, D. E., Chang, J., Malo, D. D., Carlson, C. G., Reese, C., Clay, S. A., Ellsbury, M., & Berg, B. (2001). Factors influencing spatial variability of soil apparent electrical conductivity. *Communications in Soil Science and Plant Analysis, 32*(19–20), 2993–3008.

CONOCO, (1989). Stratigraphic Lexicon and explanatory notes to the geological map of Egypt 1:500,000. In M. H. Eberhardklitzsch, F. K. List (Eds.), (pp. 263). Cairo: CONOCO Inc., ISBN 3-927541-09-5.

Corwin, D. L., Werle, J. W., & Rhoades, J. D. (1988). The use of computer assisted mapping techniques to delineate potential areas of salinity development in soils: I. A conceptual introduction. *Hilgardia, 56*(2), 1–17.

Corwin, D., Sorensen, M., & Rhoades, J. (1989). Field-testing of models which identify soils susceptible to salinity development. *Geoderma, 45*, 31–64.

Dobos, E., Norman, B., Bruee, W., Luca, M., Chris, J.,& Erika, M. (2002). The use of DEM and satellite images for regional scale soil database. In *17th World congress of soil science (WCSS)* (pp. 14–21). August 2002, Bangkok, Thailand.

El-Dars, F. M., Salem, W. A., & Fahim, M. M. (2014). Soil spatial variability in arable land south of Lake Idku, north-west Nile Delta, Egypt. *Environmental Science: An Indian Journal, 9*(10), 325–344.

FAO (1988). World agriculture toward 2000: an FAO study. In N. Alexandratos (ed.). London: Bellhaven Press. 338 pp.

FAO (2009). Advances in the assessment and monitoring of salinization and status of biosaline agriculture. Reports of expert consultation held in Dubai, United Arab Emirates, 26–29 Nov 2007. *World Soil Resources reports no 104*. Rome: FAO. 72 pp.

Farifteh, J., Farshad, A., & George, R. (2006). Assessing salt-affected soils using remote sensing, solute modelling, and geophysics. *Geoderma, 130*(3), 191–206.

Farifteh, J., Van der Meer, F., Atzberger, C., & Carranza, E. (2007). Quantitative analysis of salt-affected soil reflectance spectra: a comparison of two adaptive methods (PLSR and ANN). *Remote Sensing of Environment, 110*(1), 59–78.

Fourati, H. T., Bouaziz, M., Benzina, M., & Bouaziz, S. (2015). Modeling of soil salinity within a semi-arid region using spectral analysis. *Arabian Journal of Geosciences, 8*, 11175–11182.

Furby, S. L., Vallace, J. F., Caccetta, P. A., & Wheaton, G. A. (1995). Detecting and monitoring salt-affected land: a report from the LWRRDC project detecting and monitoring changes in land condition through time using remotely sensed data. *Remote Sensing and Image Integration Group*, CSIRO Division of Mathematics & Statistics, Western Australia.

Gandhi, G. M., Parthiban, S., Thummalu, N., & Christy, A. (2015). Ndvi: vegetation change detection using remote sensing and GIS—a case study of Vellore district. *Procedia Computer Science, 57*, 1199–1210.

Gorji, T., Tanik, A., & Sertel, E. (2015). Soil salinity prediction, monitoring and mapping using modern technologies. *Procedia Earth and Planetary Science, 15*, 507–512.

Hegab, I. A. (2014). Restrictions of bordering Idku lake low soil productivity, north Nile Delta. *Soil Science and Agriculture Engineering, 5*(2), 157–167.

Islam, S. N. (2016). Deltaic floodplains development and wetland ecosystems management in the Ganges–Brahmaputra–Meghna Rivers Delta in Bangladesh. *Sustainable Water Resources Management, 2*(3), 237–256.

Jiang, H., Shu, H., Lei, L., & Xu, J. (2017). Estimating soil salt components and salinity using hyperspectral remote sensing data in an arid area of China. *Journal of Applied Remote Sensing, 11*(1), 016043–016043.

Kihoro, J., Bosco, N. J., & Murage, H. (2013). Suitability analysis for rice growing sites using a multicriteria evaluation and GIS approach in great Mwea region, Kenya. *SpringerPlus, 2*, 265

https://springerplus.springeropen.com/track/pdf/10.1186/2193-1801-2-265?site=springerplus.springeropen.com.

Lee, K. S., Lee, G. B., & Tyler, J. (1988). Determination of soil characteristics from thematic mapper data of a cropped organic- inorganic soil landscape. *Soil Science Society of America, 52*, 1100–1104.

Lesch, S. M., Strauss, D. J., & Rhoades, J. D. (1995). Spatial prediction of soil salinity using electromagnetic induction techniques: 1. Statistical prediction models: a comparison of multiple linear regression and cokriging. *Water Resources Research, 31*, 373–386.

Mokarram, M., Hojjati, M., Roshan, G., & Negahban, S. (2015). Modeling the behavior of vegetation indices in the salt dome of Korsia in North-East of Darab, Fars, Iran. *Modeling Earth Systems and Environment, 1*(3), 1–27.

Peng, W. (1998). Synthetic analysis for extracting information on soil salinity using remote sensing and GIS: a case study of Yanggao basin in China. *Environmental Management, 22*(1), 153–159.

Perkins, T., Adler-Golden, S., Matthew, M., Berk, A., Anderson, G., Gardner, J., & Felde, G. (2005). Retrieval of atmospheric properties from hyper and multispectral imagery with the FLAASH atmospheric correction algorithm. In: K. Schäfer, A. T. Comerón, J. R. Slusser, R. H. Picard, M. R. Carleer, N. Sifakis (Eds.), *Remote sensing of clouds and the atmosphere X*. Proceedings of SPIE vol. 5979.

Pozdnyakova, L., & Zhang, R. (1999). Geostatistical analyses of soil salinity in a large field. *Precision Agriculture, 1*, 153–165.

Robinson, T., & Metternicht, G. (2006). Testing the performance of spatial interpolation techniques for mapping soil properties. *Computers and Electronics in Agriculture, 50*, 97–108.

Saaty, T. L. (1980). *The analytic hierarchy process: planning, priority setting, resources allocation* (p. 287). London: McGraw-Hill.

Shahid, S. A. (2013). Developments in soil salinity assessment, modeling, mapping, and monitoring from regional to submicroscopic scales. In *Developments in soil salinity assessment and reclamation* (pp. 3–43). Springer.

Sharma, D., & Singh, A. (2017). Current trends and emerging challenges in sustainable management of salt-affected soils: a critical appraisal. In S. Arora, A. Singh, & Y. Singh (Eds.), *Bioremediation of salt affected soils: an Indian perspective* (pp. 1–40). Cham: Springer.

Thornbury, W. D. (1950. Glacial sluiceways and lacustrine plains of southern Indiana. Bulletin no. 4. In *Division of Geology, Indiana Department of Conservation, Bloomington, Indiana*. 21pp.

USDA. (2004). *Soil survey laboratory methods manual*. Soil Survey Investigation Report No. 42 Version 4.0 November, USA.

USDA. (2014). *Keys to soil taxonomy*, 12th edn. United States Department of Agriculture, Natural Resources Conservation Service (NRCS), USA. 362pp.

Wu, W., Mhaimeed, A., Al-Shafie, W., Ziadat, F., Dhehibi, B., Nangia, V., & Pauwa, E. (2014). Mapping soil salinity changes using remote sensing in Central Iraq. *Geoderma Regional, 2*, 21–31.

Yahiaoui, I., Douaoui, A., Zhang, Q., & Ziane, A. (2015). Soil salinity prediction in the Lower Cheliff plain (Algeria) based on remote sensing and topographic feature analysis. *Journal of Arid Land, 7*, 794–805.

Yengoh, G. T., Dent, D., Olsson, L., Tengberg, A. E., & Tucker, C. J. (2014). *The use of the normalized difference vegetation index (NDVI) to assess land degradation at multiple scales: a review of the current status, future trends, and practical considerations*. Sweden: Lund University Centre Report for Sustainability Studies.

Yin, H., Dang, Y., Xue, S., Wang, Q., & Yi, H. (2012) An improved inverse distance weighted method for interpolating ZTD based on regional GPS network. In *Paper presented at the China Satellite Navigation Conference (CSNC) 2012 Proceedings* (pp. 463–471). Springer.

Yu, H., Liu, M., Du, B., Wang, Z., Hu, L., & Zhang, B. (2018). Mapping soil salinity/sodicity by using Landsat OLI imagery and PLSR algorithm over semiarid West Jilin Province. *China Sensors, 18*, 1048.

Zaki, A., & Swelam, A. (2017). The climatology of Nile Delta, Egypt. *International Center for Agricultural Research in the Dry Areas (ICARDA)* (pp. 1–32).

Zewdu, S., Suryabhagavan, K., & Balakrishnan, M. (2017). Geospatial approach for soil salinity mapping in Sego Irrigation Farm, South Ethiopia. *Journal of the Saudi Society of Agricultural Sciences, 16*(1), 16–24.

Zinck, J. A., & Valenzuela, C. R. (1990). Soil geographic database: structure and application examples. *ITC journal, 3*, 270–294.